IEEE Access
Multidisciplinary ⋮ Rapid Review ⋮ Open Access Journal

Received 29 November 2022, accepted 9 January 2023, date of publication 16 January 2023, date of current version 1 February 2023.

Digital Object Identifier 10.1109/ACCESS.2023.3237511

RESEARCH ARTICLE

A Novel DPC Approach for DFIG-Based Variable Speed Wind Power Systems Using DSpace

HAMID CHOJAA[1], AZIZ DEROUICH[1], OTHMANE ZAMZOUM[1], SAID MAHFOUD[1], MOHAMMED TAOUSSI[1], HANI ALBALAWI[2,3], (Member, IEEE), HABIB BENBOUHENNI[4], AND MOHAMED I. MOSAAD[5,6], (Senior Member, IEEE)

[1]Industrial Technologies and Services Laboratory, Higher School of Technology, Sidi Mohamed Ben Abdellah University, Fez 30000, Morocco
[2]Department of Electrical Engineering, Faculty of Engineering, University of Tabuk, Tabuk 47512, Saudi Arabia
[3]Renewable Energy and Energy Efficiency Center (REEEC), University of Tabuk, Tabuk 47512, Saudi Arabia
[4]Department of Electrical and Electronics Engineering, Faculty of Engineering and Architecture, Nisantasi University, 34481742 İstanbul, Turkey
[5]Department of Electrical Engineering, Faculty of Engineering, Damietta University, Damietta 34517, Egypt
[6]Yanbu Industrial College (YIC), Alnahdah, Yanbu Al Sinaiyah, Yanbu 46452, Saudi Arabia

Corresponding authors: Hamid Chojaa (chojaa.hamid@gmail.com) and Mohamed I. Mosaad (m_i_mosaad@hotmail.com)

ABSTRACT The integration of wind energy systems into the electric grid has become inevitable despite the many problems associated with this integration. Most of these problems are due to variations in wind speed. The problems are for example oscillations in the power generated, which implies the lack of guarantee of obtaining the maximum energy and the ripple in the electromechanical torque of the generator. This work aims at mitigating these problems for wind energy conversion system-driven doubly-fed induction generator (DFIG), which is the main wind turbine utilized for energy applications. This mitigation is performed through direct reactive and active powers control of the DFIG using an artificial neural network. A DSP (Digital Signal Processor-dSPACE DS1104) was used to experimentally test the proposed strategy. The dynamic performances of the controlled generator are analyzed by using the designed intelligent control strategy in the case of variable wind speeds and upon sudden change of the active power demand. Based on the obtained experimental results, it can be said that the designed intelligent control strategy outperforms traditional methods like direct power (DPC) and vector control in terms of reducing the current harmonics, and torque ripples, and enhancing dynamic response.

INDEX TERMS Artificial neural network, direct power control, DFIG, digital signal processor, variable wind speeds.

I. INTRODUCTION

Developing and increasing the utilization of renewable energy sources had become necessary thanks to the low cost of these sources, and their impact on reducing gas emissions. Due to its technological development, wind power has become the most widely used and popular type compared to other renewable energy sources. This is because of the ease of control and the reasonable production cost of electrical energy [1]. The problem associated with using wind energy as a source of energy is the full dependence on the wind speed which is variable. This speed variation negatively affects the quality of the generated power since it causes fluctuations in the electrical power, and ripples in the electromagnetic torque of the generator besides the deviation from the maximum point of the produced power from wind turbine systems (WTSs) [2]. Dealing with variable-speed WTS is a challenging and complex issue that leads to the continued use of fixed-speed WTS despite its drawbacks [2], [3]. On the other hand, variable-speed WTS acquire accurate and efficient control algorithms to deal with these variations in the generated energy and to maintain the energy quality at higher levels. The critical issue before selecting and designing the controller is choosing the appropriate generator for such variable-speed applications [4]. The most suitable generator for such applications is the doubly-fed induction generator (DFIG) [5]. DFIGs represent more than 50% of the generators used in WTSs [6] although the presence of

The associate editor coordinating the review of this manuscript and approving it for publication was Feng Wu.

This work is licensed under a Creative Commons Attribution-NonCommercial-NoDerivatives 4.0 License.
For more information, see https://creativecommons.org/licenses/by-nc-nd/4.0/

other generators like switched reluctance generators [7], self-excited asynchronous generators [8], and permanent magnet synchronous generators [9]. DFIGs are characterized by durability, low maintenance cost, and ease of control compared to other types [10]. In addition, there are many control schemes of DFIG-WTS. The classic control scheme is a field-oriented control (FOC) that is widely used in industrial applications [11]. However, the implementation of the FOC strategy to regulate DFIG power still suffers from the disadvantages of ripples in torque, active power, and slow dynamic response due to the use of a proportional-integral (PI) controller [12]. Moreover, the performance of the FOC strategy depends largely on the accuracy of the studied model compared to other controls. In addition, the dynamic performance of DFIG-based WTS controlled by the FOC strategy strongly depends on the design of the PI parameters. The PI parameters of the FOC strategy are proposed based on a single operating point [13]. In other words, the PI controller can not adapt its parameters if the operating point is changed [14].

Several techniques have been suggested to replace the FOC strategy and advance the dynamic response of electric machines. Direct torque control (DTC) is one of the most popular and simplest of these techniques [15]. DTC was used for the first time in order to control the asynchronous motor and then it was applied to all electrical machines [16]. This control is among the least expensive and gives a very fast dynamic response compared to the FOC strategy [17]. There is another control with the same principle as the DTC strategy, and this technique uses also a switching table to control the inverter. Direct power control (DPC) is the name of this control method, and it possesses the same features and advantages as the DTC strategy [18]. The difference between DPC and DTC strategies is the reference magnitudes used in control, wherein DTC strategy, torque, and flux are used. But reactive and active power are employed as references in DPC.

The use of DPC to manage the field of control allowed for the asynchronous and the synchronous generators, due to the simplicity of control, straightforward to implement, and inexpensive of completion compared to classical controls such as FOC [19]. Moreover, due to the dynamic response offered by this strategy, unlike other controllers. FOC has numerous benefits and distinguishing features, but there are also a number of defects such as many ripples in both the reactive and active power. As well as the low quality of the current generated, it results in a reduction in the life of electrical appliances. To avoid these problems and try to reduce them, there are several solutions suggested to advance the effectiveness and the operation of the DPC. Among these solutions, we find artificial intelligence and nonlinear techniques [20], [21]. These techniques gave good results, especially in terms of dynamic response. However, they require proficiency to change their parameters as they gain greater expertise and take longer to adjust.

Several experimental works were carried out on the DFIGs to verify the designed methods as summarized in Table 1.

TABLE 1. Experimentally implemented methods on DFIGs.

Rating (kW)	Technique	Controller	Current oscillations	complexity	Reference Tracking *	Reference
2.25	DPC	Neural algorithm	Neglected	High	+++	[22]
3500	FOC strategy	Hysteresis rotor current controller	Low	Medium	++	[23]
15	FOC strategy	PI	High	Low	++	[24]
2	DPC	SMC	Low	Medium	+++	[25]
7.5	Direct FOC strategy	PI controller	High	High	++	[26]
7	Nonlinear control	second-order sliding-mode control	Low	High	+++	[27]
1	Nonlinear control	integral sliding mode controller	High	High	++	[28]
11	FOC strategy with a full-order adaptive observer	PI	High	Low	++	[29]
3	FOC strategy with space vector modulation	PI	High	Low	++	[30]
1.5	Predictive Current Control	-	High	Low	++	[31]
2.2	Vector control	PI	High	Low	++	[32]
10	Deadbeat predictive control	-	High	Low	++	[33]
10	voltage-oriented control with limited-position set model-reference adaptive observer	PI	High	Medium	++	[34]

* + medium ++ high +++ very high

Through this table, several techniques have been experimentally implemented, including what is linear and non-linear, and this is by using several types of controllers such as PI, sliding mode controller (SMC), and synergetic controller. It should be mentioned that all the applied works were conducted using asynchronous generators with low power, where the power range is between 1 KW and 15 KW.

Through the experimental work, no control scheme gives much better results or eliminates ripples for the reactive and active powers. Moreover, the dynamic response varies from one technique to another. By comparing these experimental works, the DPC technique gives unacceptable results. In this

technique, there are ripples in both the current and the active power that gives a large value to the total harmonic distortion (THD) in the current waveform. All these defects lead to a reduction in the life of electrical appliances and fluctuations in the electrical network.

To enhance the quality of the current that is produced by the DFIG-WTS and reduce ripples at the level of current, torque and active power, a new DPC strategy is proposed and it is experimentally verified. In this experimental work, a novel idea is given for DPC strategy using both artificial neural network and pulse width modulation (PWM). The designed DPC technique is a radically modified version of the classical DPC technique, where both the switching table and hysteresis controller are replaced to get a more robust DPC strategy. The designed intelligent strategy will be explained in detail in the remainder of the work.

The contribution made in this paper can be summed up in the following statements:

1. A novel form of DPC strategy based on artificial neural networks and PWM technique.
2. Experimental implementation of the proposed intelligent DPC technique using dSPACE.
3. Reducing ripples at the level of both active power and current.

This work contains seven headings from the introduction to the references. Section I is an introduction. Section II describes the single-rotor wind turbine modeling. Section III presents the proposed intelligent DPC strategy using PWM technique. Numerical results are described in Section IV of the paper. The implementation of the proposed technique using the DSPACE card is explained in detail in Section V. Section VI describes the experimental results obtained from the designed intelligent control using variable and step speed wind profiles. Finally, this experimental work was ended with a conclusion, where all the conclusions reached through this work were summarized.

II. MODELING OF THE WTSs

In the past years, existing electric power generation systems that have been used in wind energy were based principally on induction generators due to their high efficiency and flexible controllability. The following figure represents an electrical power generation system using wind energy. In this way, to generate electric power, we need a generator, a turbine to rotate the generator and we also need two inverters to feed the generator. To spotlight the advantages the proposed system is very simple and inexpensive compared to the traditional technique of generating electric power, and on the other hand, it contributes to reducing gaseous emissions [35].

The wind's energy can be expressed as [36]:

$$P_t = \frac{1}{2}\rho\pi R^2 V^3 C_P(\lambda, \beta) \tag{1}$$

The power produced by the wind is related to the speed of the wind (V), the blade length (R), power coefficient (C_P), and the air density (ρ), contrasted with, we can express the power

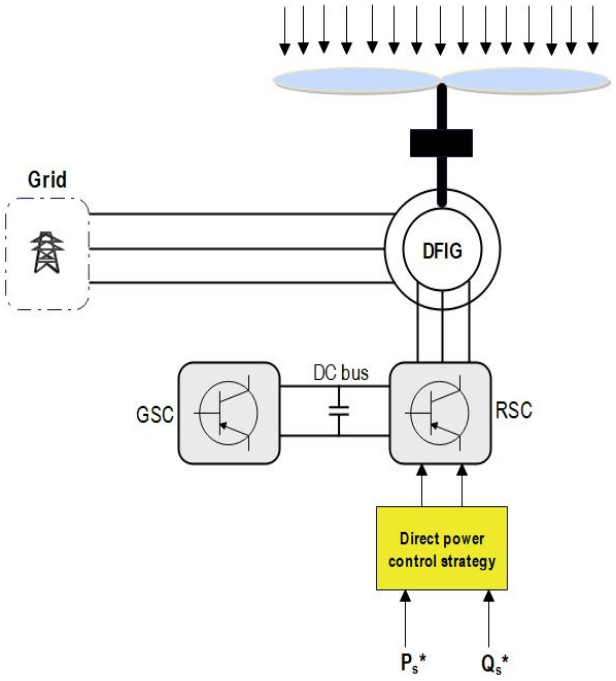

FIGURE 1. Structure of WTS.

coefficient by Equation (2).

$$Cp(\lambda, \beta) = 0.5\left(\frac{116}{\lambda i} - 0.4\beta - 5\right) exp\left(\frac{-21}{\lambda i}\right) + 0.0068\lambda \tag{2}$$

Through this equation, the value of Cp is related to (β) and the tip speed ratio (λ). The value of Cp can be controlled by changing the wind reception pitch angle (β) of the turbine blades. As is known, Cp is maximum when $\beta = 0$. Equation (3) depicts the turbine's tip speed ratio. Through this equation, the tip speed ratio is closely related to the pitch angle. According to Equation (3), λ is maximum when the pitch angle is zero, and in this case, the power gained from the wind is maximum.

$$\frac{1}{\lambda i} = \frac{1}{\lambda + 0.08\beta} - \frac{0.035}{\beta^3 + 1} \tag{3}$$

Equation (4) shows the relationship between the speed of a turbine (Ω_t), blade length, wind speed, and λ. So, the optimal value of λ can be determined as:

$$\lambda = \frac{\Omega_t R}{V} \tag{4}$$

The torque produced by the turbine can be expressed by the following equation [29]:

$$T_{aer} = \frac{1}{2\Omega_t}\rho\pi R^2 V^3 C_P(\lambda, \beta) \tag{5}$$

The function of the gearbox is to adapt the low speed Ω_t of the turbine rotor to the high speed Ω_m of the DFIG:

$$\begin{cases} T_m = \dfrac{T_{aer}}{G} \\ \Omega_m = G\Omega_t \end{cases} \tag{6}$$

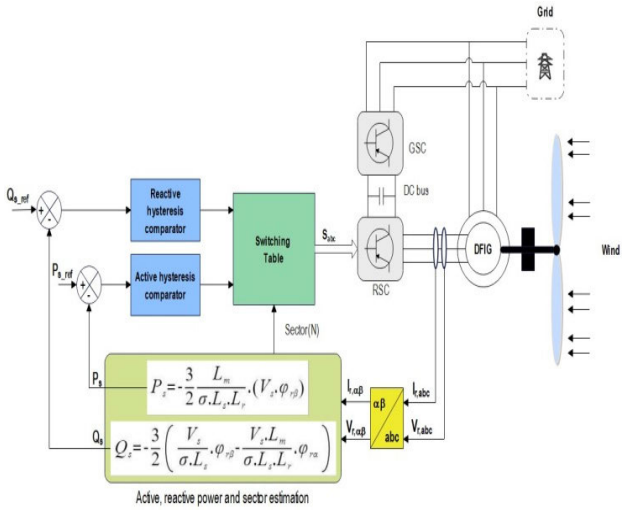

FIGURE 2. Traditional DPC strategy.

From the torque (T_{aer}) and speed (Ω_t) of the turbine, the speed (Ω_g) and torque (T_g) of the DFIG can be calculated using the equation (6).

The speed and torque of the turbine and the DFIG can be linked by the following relationship:

$$T_m - T_{em} - f \cdot \Omega_m = J_{tot} \cdot \frac{d\,\Omega_m}{dt} \tag{7}$$

where, J_{tot} is the moment of inertia and f is the total friction.

As is well known, the adopted generator (DFIG) is made up of two sections, one of which is static and the other is movable. This generator has characteristics that distinguish it from other machines or other types, as it is easy to control and gives a greater energy return if there is a changing wind speed [37]. To give the mathematical form of this type of machine (DFIG) in this work, we will give all the equations that express the voltage and flux of the generator in addition to the mechanical equation. The voltages of the rotor and stator section of the DFIG are shown in the following equation [11]:

$$\begin{cases} \mathrm{V_{ds}} = \mathrm{R_s I_{ds}} + \dfrac{\mathrm{d}}{\mathrm{dt}}\psi_{\mathrm{ds}} - \omega_{\mathrm{s}}\psi_{\mathrm{qs}} \\ \mathrm{V_{qs}} = \mathrm{R_s I_{qs}} + \dfrac{\mathrm{d}}{\mathrm{dt}}\psi_{\mathrm{qs}} + \omega_{\mathrm{s}}\psi_{\mathrm{ds}} \\ \mathrm{V_{dr}} = \mathrm{R_r I_{dr}} + \dfrac{\mathrm{d}}{\mathrm{dt}}\psi_{\mathrm{dr}} - \omega_{\mathrm{r}}\psi_{\mathrm{qr}} \\ \mathrm{V_{qr}} = \mathrm{R_r I_{qr}} + \dfrac{\mathrm{d}}{\mathrm{dt}}\psi_{\mathrm{qr}} + \omega_{\mathrm{r}}\psi_{\mathrm{dr}} \end{cases} \tag{8}$$

Equation(9) represents the flux at the stator and rotor level.

$$\begin{cases} \psi_{ds} = L_s I_{ds} + M I_{dr} \\ \psi_{qs} = L_s I_{qs} + M I_{qr} \\ \psi_{dr} = L_r I_{dr} + M I_{ds} \\ \psi_{qr} = L_r I_{qr} + M I_{qs} \end{cases} \tag{9}$$

where, i_{sd}, i_{sq}, i_{rd}, i_{rq}, are the stator and rotor d-q axes currents, respectively. ϕ_{sd}, ϕ_{sq}, ϕ_{rd}, ϕ_{rq}, are the stator and rotor flux components, respectively. V_{sd}, V_{sq}, V_{rd}, V_{rq}, are the d-q axes voltage components of the stator and rotor, respectively.

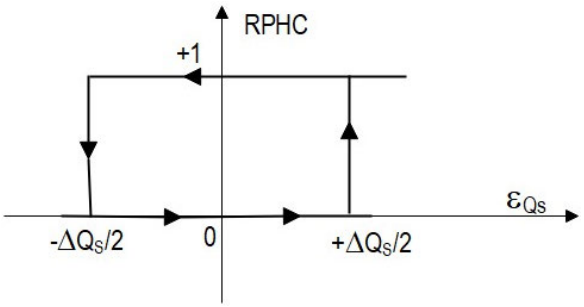

FIGURE 3. Reactive power hysteresis comparator.

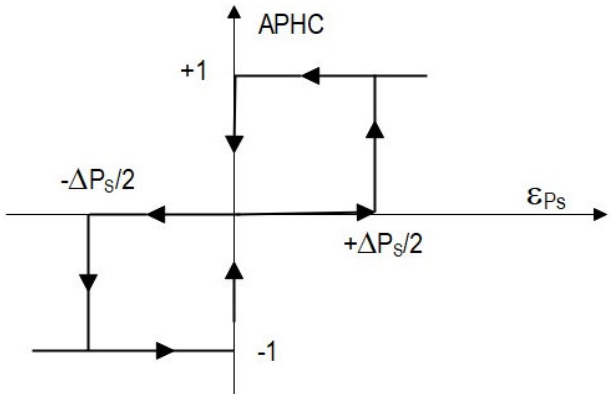

FIGURE 4. Active power hysteresis comparator.

The active power of the DFIG is the product of the current and the voltage, and the same magnitudes define the reactive power. Equation (10) represents the relationships that determine the reactive and active power of the DFIG.

$$\begin{cases} P_s = \dfrac{3}{2}(V_{ds} I_{ds} + V_{qs} I_{qs}) \\ Q_s = \dfrac{3}{2}(V_{qs} I_{ds} - V_{ds} I_{qs}) \end{cases} \tag{10}$$

The mathematical form of the DFIG is not complete without the mechanical part model. The latter can be expressed by equation (11). The mechanical component depicts how torque and speed of the DFIG are related [13].

$$T_e - T_r = J \cdot \frac{d\Omega}{dt} + f \cdot \Omega \tag{11}$$

In the control, there are several techniques used to control generators, and the most famous of these techniques are the non-linear ones that depend on the use of SMC. This control is more robust than the DTC, FOC, and the DPC strategies. The DFIG control in this paper is dealt with using the proposed DPC strategy, and this depends on the maximum power point tracking (MPPT) strategy.

III. PROPOSED DPC STRATEGY

The DPC has historically been utilized extensively in the production of renewable energy because of its benefits in

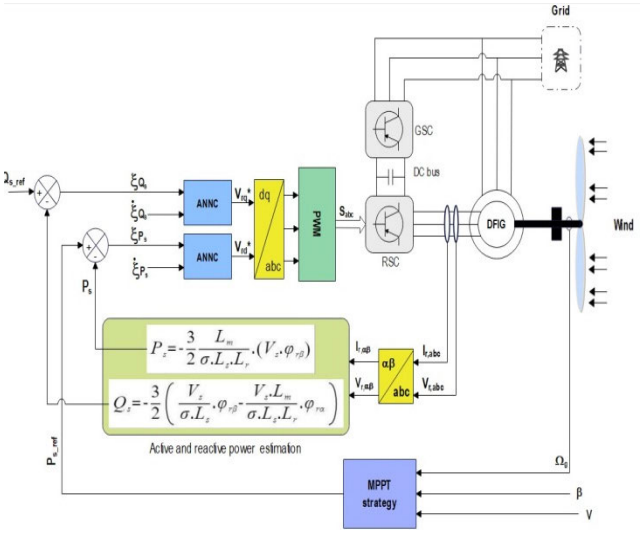

FIGURE 5. The proposed control of the DFIG-WTS.

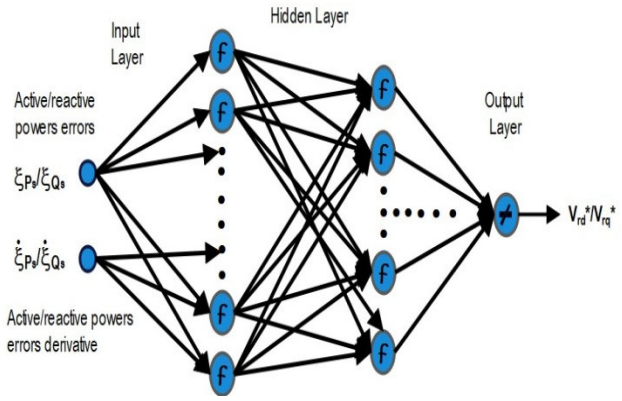

FIGURE 6. The internal architectures of the utilized MLPs.

terms of dynamic responsiveness, quick and easy implementation. [38]. However, classical DPC using a lookup table is a robust strategy compared to the FOC technique. In this control, the inverter is controlled using a lookup table and two hysteresis comparators are used to regulate the active and reactive powers [39]. Figure 2 shows the classical DPC for controlling a WTS driven by a DFIG. From this figure, the DPC is a simple strategy that minimized current undulations, reactive/active power undulations, and THD of voltage/current compared to the FOC strategy. Comparing this method to vector control, it also provides a quick reaction dynamic [40].

In this technique, to regulate the reactive and active power, we need to estimate both the quadrature and direct rotor flux of the DFIG. The rated values of quadrature and direct rotor flux are used to calculate the values for the rated active and reactive power. These values are called measured values that are used as the reference values for calculating the errors in active and reactive powers. Equation (12) represents how to calculate each of the quadrature and direct rotor fluxes

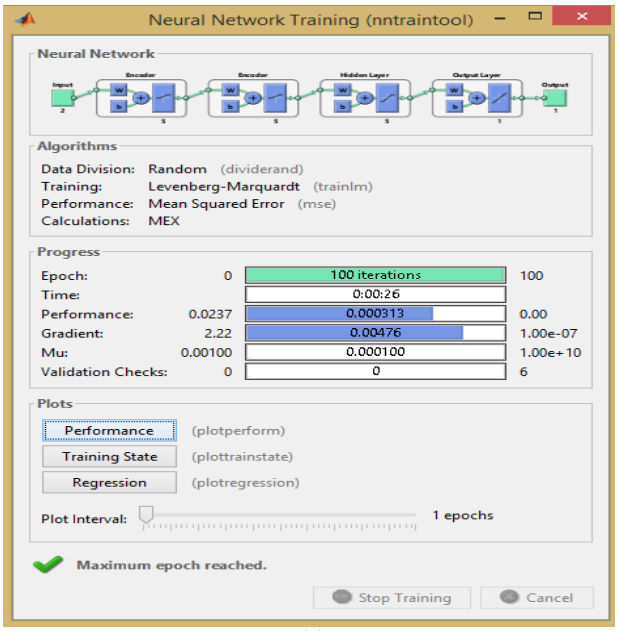

(a)

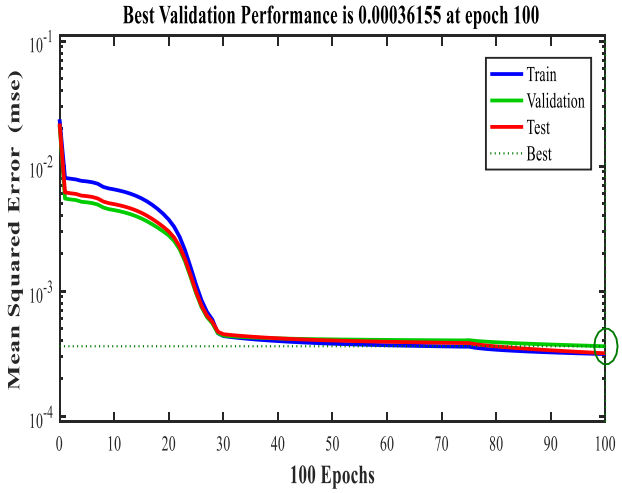

(b)

FIGURE 7. (a) Active power controller ANN learning development and training (b) Performance curve of training (MSE).

of the DFIG. Through this equation, it can be said that the quadrature and direct rotor flux is related to the values of both rotor voltage and current.

$$\begin{cases} \Psi_{r\alpha} = \int_0^t (V_{r\alpha} - R_r\, I_{r\alpha})dt \\ \Psi_{r\beta} = \int_0^t (V_{r\beta} - R_r\, I_{r\beta})dt \end{cases} \tag{12}$$

The flux amplitude is calculated by:

$$\Psi_r = \sqrt{\Psi_{r\alpha}^2 + \Psi_{r\beta}^2} \tag{13}$$

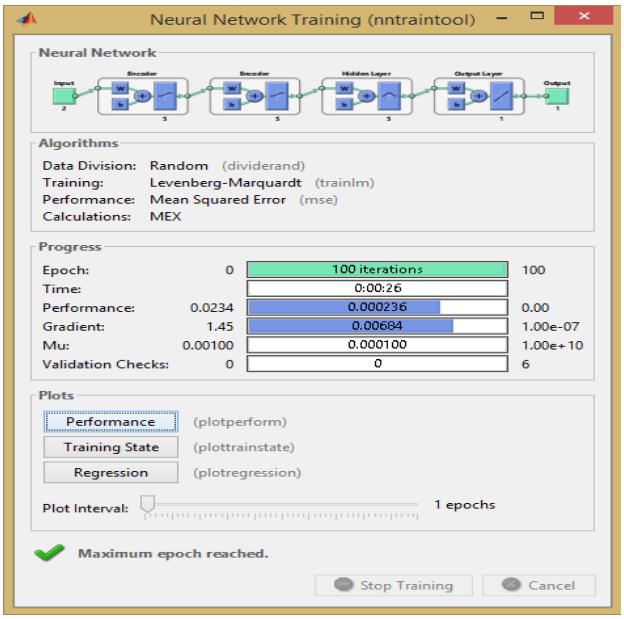

(a)

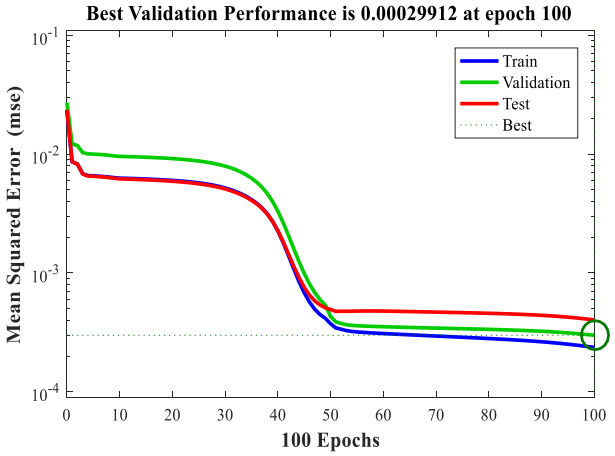

(b)

FIGURE 8. (a) React power controller ANN learning development and training (b) Performance curve of training (MSE).

The rotor flux and voltage interrelationship is shown in Equation (14).

$$\left|\overline{\Psi_r}\right| = \frac{\left|\overline{V_r}\right|}{w_r} \tag{14}$$

Equation (15) represents the rotor flux angle, where this angle is employed to determine the locations where the reference voltage ray is present. This perspective is crucial in understanding. This angle has a countless significance in traditional direct control of torque and power.

$$\theta_r = arctg(\frac{\Psi_{r\beta}}{\Psi_{r\alpha}}) \tag{15}$$

To calculate the value of each of the active and reactive power, equations (16) and (17) can be used. Through these two equations, the value of the reactive and active power is related to the value of quadrature and direct stator voltage and rotor flux [13].

$$P_s = -\frac{3}{2}\frac{Lm}{\sigma.Ls.Lr} \cdot (Vs.\psi_{r\beta}) \tag{16}$$

$$Q_s = -\frac{3}{2}(\frac{Vs}{\sigma.Ls} \cdot \psi_{r\beta} - \frac{Vs.Lm}{\sigma.Ls.Lr} \cdot \psi_{r\alpha}) \tag{17}$$

With:

$$\sigma = 1 - \frac{M^2}{L_r\, L_s} \tag{18}$$

As is known, to control the inverter, a switching table employed in the DTC is used. On the other hand, two hysteresis controllers are presented to control the reactive and active power. A two-level hysteresis controller was used to regulate the reactive power, and a three-level hysteresis controller was used to regulate the active power. Figure 3 shows the reactive power hysteresis comparator (RPHC), where this exists as the last output gives the last two values 0 and 1. In addition, the output of the active power hysteresis comparator (APHC) is 0, 1, and −1 (see Figure 4). In addition, the output of reactive and active power hysteresis controllers is the input of the traditional lookup table. The zone of the rotor flux is six-zone and the classical lookup table is provided in Table 2, [39]. In the traditional DPC strategy, there are 8 voltages (V0 to V7) generated by the classical inverter, and these voltages are used to fill in a classical lookup table. Moreover, there are 6 zones of the reference voltage.

TABLE 2. Lookup table of traditional DPC strategy.

N		1	2	3	4	5	6
RPHC	APHC						
0	1	6	1	2	3	4	5
	0	0	7	0	7	0	7
	-1	2	3	4	5	6	1
1	1	5	6	1	2	3	4
	0	7	0	7	0	7	0
	-1	3	4	5	6	1	2

The traditional DPC technique of the DFIG has downsides like any other strategy. It gives better results compared to the FOC strategy. But there are ripples at the level of both the reactive and active power, and the value of the current THD is high, which leads to poor quality of the current and thus the effect on the network [42]. All this leads to a weakening of the efficiency of electrical machines and a shortening of the life of the equipment. Additionally, the current's poor-quality results in a lot of faults, and consequently, the high cost of maintenance [43].

To address the shortcomings of the conventional DPC strategy, a novel control was proposed in this study. The designed methodology is based on ANN and PWM techniques. The designed technique is a robust/simple technique, simple to implement, and has a dynamic quick response dynamic compared to the DPC and FOC strategies. This suggested controller is a radical modification of the DPC, where the PWM

TABLE 3. ANN parameters.

ANN parameters	Value/methods	
	ANNC-P_s	ANNC-Q_s
Neural network	MLP network	
MLP training process	Levenberg Marquardt algorithm	
Proposed structure	2-5-5-5-1	2-5-5-5-1
Number of repetitions	100	100
Input layer	ξ_{Ps} and $\dot{\xi}_{Ps}$	ξ_{Qs} and $\dot{\xi}_{Qs}$
Output layer	V_{rq_ref}	V_{rd_ref}
Activation functions	Tansig	Tansig
Adaption learning function	Trainlm	Trainlm

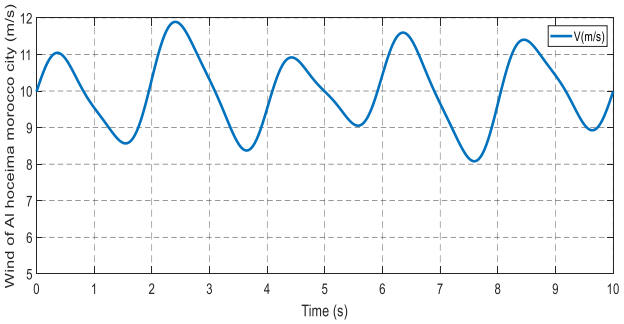

FIGURE 9. Wind profile.

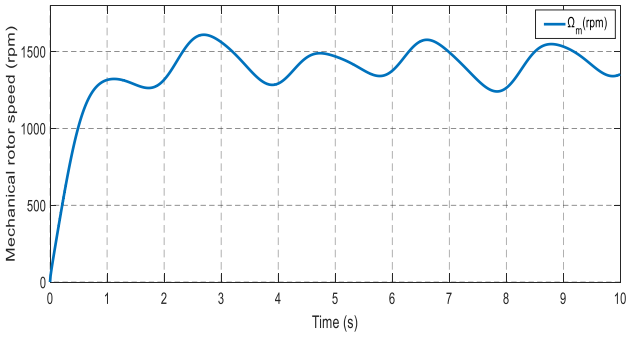

FIGURE 10. Mechanical rotor speed.

technique is utilized instead of a classical lookup table and ANN controllers are used instead of a hysteresis comparator. In this way, a more robust technique is obtained compared to both the DPC and FOC strategies.

Figure 5 depicts the planned DPC technique that is suggested for regulating the reactive and active powers of the DFIG-based variable speed WTS.

In this presented strategy, an ANN controller was used for regulating the reactive and active powers. This control, as is well known, is one of the most often used artificial intelligence controllers. This control was used to obtain a high quality of the electric current produced by the DFIG, and to minimize the fluctuations of the current, active power, and torque. Furthermore, we can get with the technique a minimum value of THD of current. The coefficients of the ANN controllers presented in this work are given in Table 3.

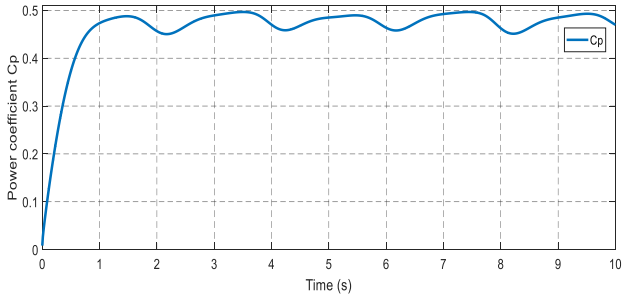

FIGURE 11. Power coefficient.

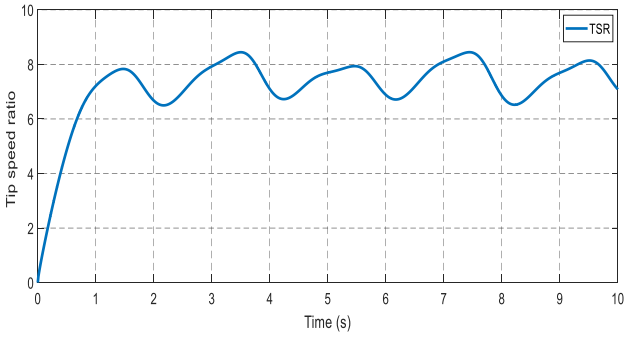

FIGURE 12. Tip speed ratio.

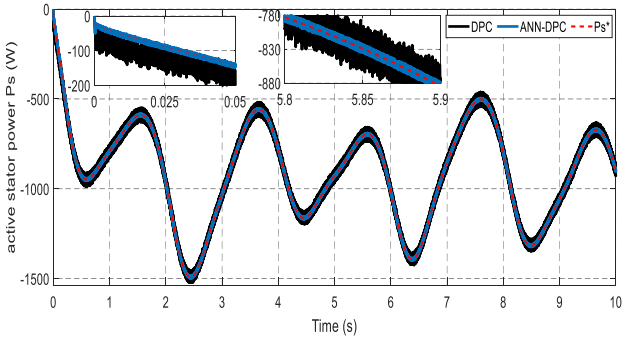

FIGURE 13. Active power.

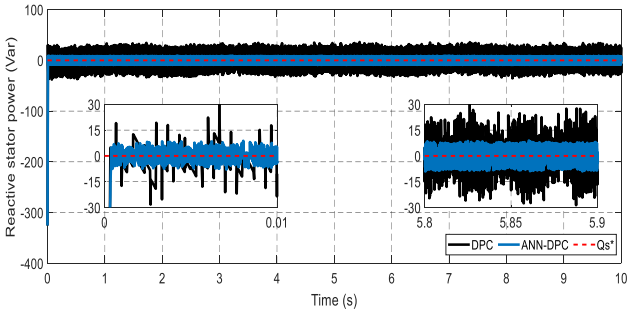

FIGURE 14. Reactive power.

The characteristic equation of the neuron in the l^{th} layer is presented in Equation (19) [38].

$$Y_j^l = f\left(\sum_i^{nl} W_{ji}^l X_i + b_j^l\right) \tag{19}$$

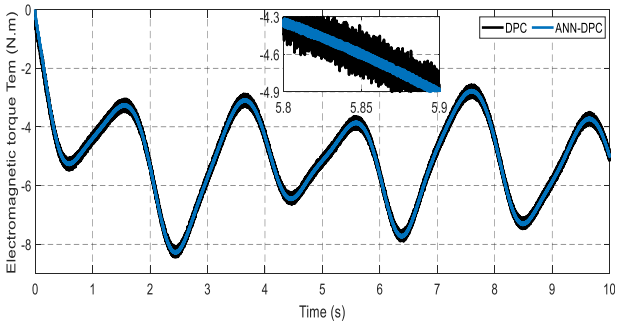

FIGURE 15. Electromagnetic torque.

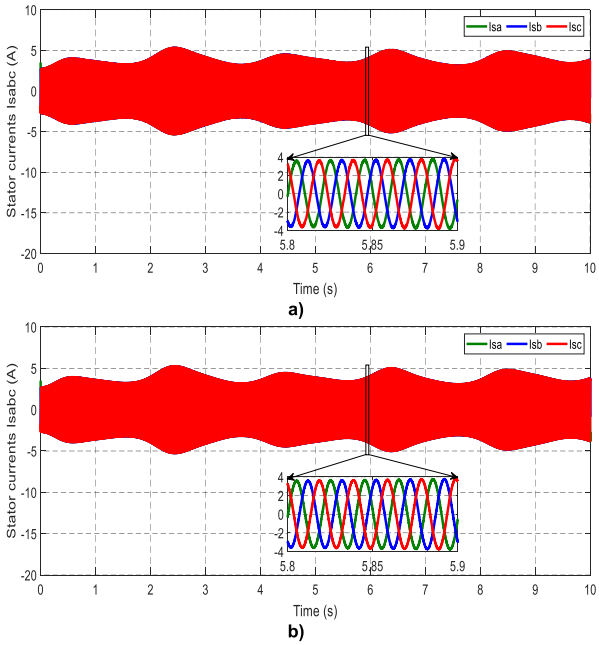

FIGURE 16. Stator currents isabc of both methods: (a) DPC and (b) ANNDPC.

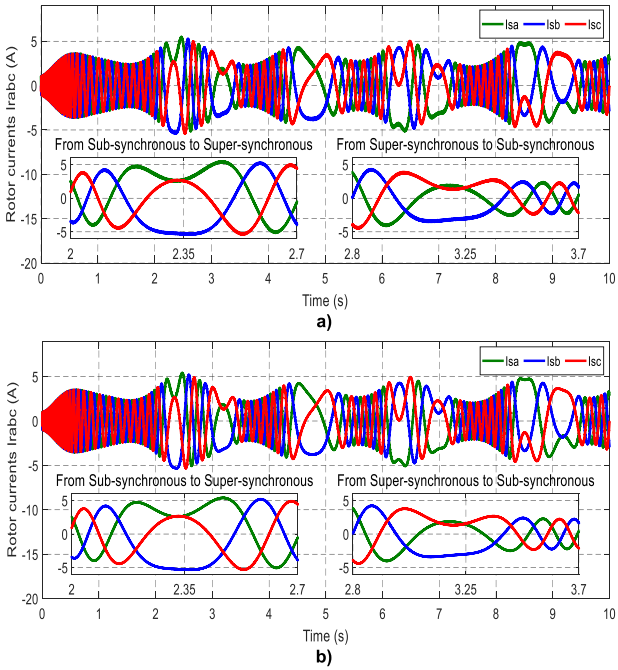

FIGURE 17. Rotor current irabc of both methods: (a) DPC and (b) ANN-DPC.

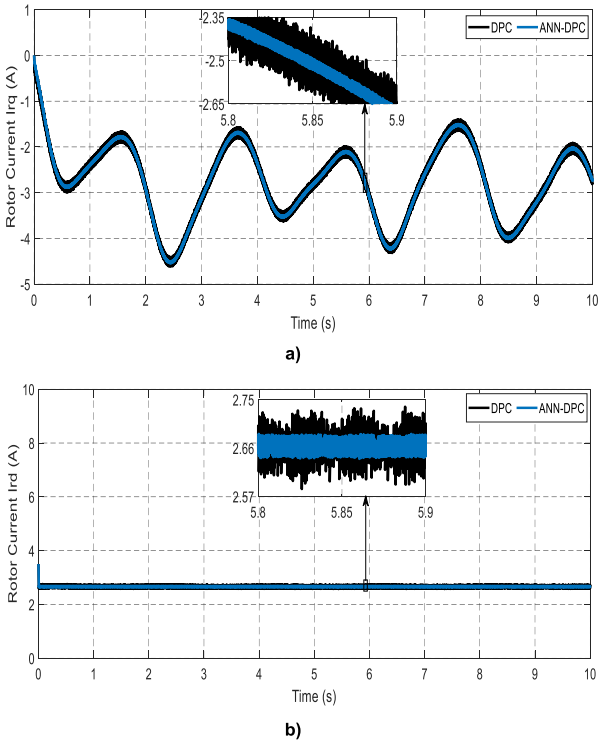

FIGURE 18. Direct and quadrature rotor currents: a) i_{rq}, b) i_{rd}.

where, X_i is the inputs vector, W_{ji}^{l} is the synaptic weights of neuron j in layer l and b_j^l: bias input.

The proposed ANN controllers have been selected to be static MLPs, and the architectural schemes of the employed (MLPs) are displayed in Figure 6. The two used MLPs controllers have consisted of an input layer with two neurons representing power active error (ξ_{Ps}) and its derivative ($\dot{\xi}_{Ps}$), and power reactive error (ξ_{Qs}) and its derivative ($\dot{\xi}_{Qs}$) successively, two hidden layers, and an output layer with one neuron representing the rotor voltage reference components V_{rq_ref} and V_{rd_ref} successively [38].

Figures 7a and 8a, show how active and reactive power controllers are evolving in terms of learning. It should be noticed that the suggested architectures (2-5-5-5-1) for the reactive and active powers controllers swiftly reach the finest outcome as of the 30th and 50th iterations, respectively.

It should be noted that during the 100th iteration, the Mean Square Error (MSE) for both controllers is seen to have a tiny value, reaching 3.62 $\times 10^{-4}$ and 3.69 $\times 10^{-}$ for each controller.

IV. SIMULATION RESULTS

The presented technique is applied to a DFIG (1.5 KW) and all these simulations were performed using Matlab/Simulink

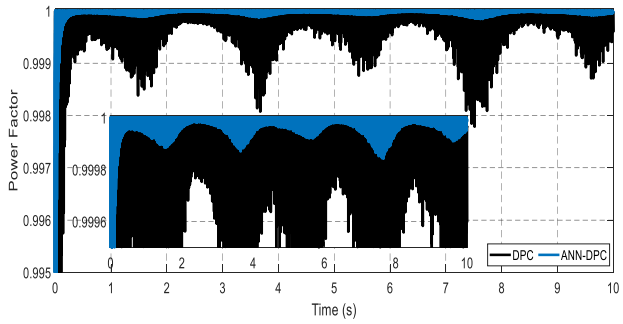

FIGURE 19. Power factor.

TABLE 4. System parameters.

Parameters OF WIND TURBINE AND GENERATOR			
Parameters	**Value**	**Parameters**	**Value**
Number of blades	3	Rotor current, I_{rn} (A)	8.5
Rotor radius R (m)	1	Number of pair of poles, p	2
Gearbox gain G	2	Stator rated frequency, f_s (Hz)	50
Friction coefficient f (N.m.s/rad)	0.0027	Stator resistance, R_s (Ω)	1.18
Moment of inertia J ($kg.m^2$)	0.04	Rotor resistance, R_r (Ω)	1.66
Rated power, P_n (KW)	1.5	Stator inductance, L_s (H)	0.20
Stator rated voltage, V_s (V)	220 / 380	Rotor Inductance, L_r (H)	0.18
Stator current, I_{sn} (A)	5.2	Mutual inductance, M (H)	0.17

software. The parameters of the DFIG utilized in this study are tabulated in Table 4.

In this part, two test cases are projected to evaluate the durability of the proposed technique, where the first test case is a step-change in the wind speed and the second case is a variable wind speed profile. These two test cases aim to study the behavior of the proposed technique compared to the change of references.

A. FIRST TEST CASE

The first test case is to use variable wind speed to study the behavior of the designed control under the effect of changing wind speed. In this case, the wind behavior was used in the Moroccan city of Al Hoceima as illustated in Figure 6. The findings of this test are shown in Figures 7 to 16. Figure 7 depicts the mechanical speed of the generator. According to this figure, speed is erratic and manifests as a shift in the wind. Additionally, the minimum and maximum rotor speeds are 1250 rpm and about 1550 rpm, respectively.

The power coefficient (Cp) is plotted. As it is noticed that the profile of Cp change is the same as the profile of wind speed change, the change in wind speed has an impact on this value. The turbine's λ is plotted in Figure 9.

The reactive and active power precisely follow the references in Figures 10 and 11 respectively. The active power manifests as a shift in wind speed, with the value of the active power increasing while wind speed increases and vice versa. The reactive power is zero in accordance with the chosen

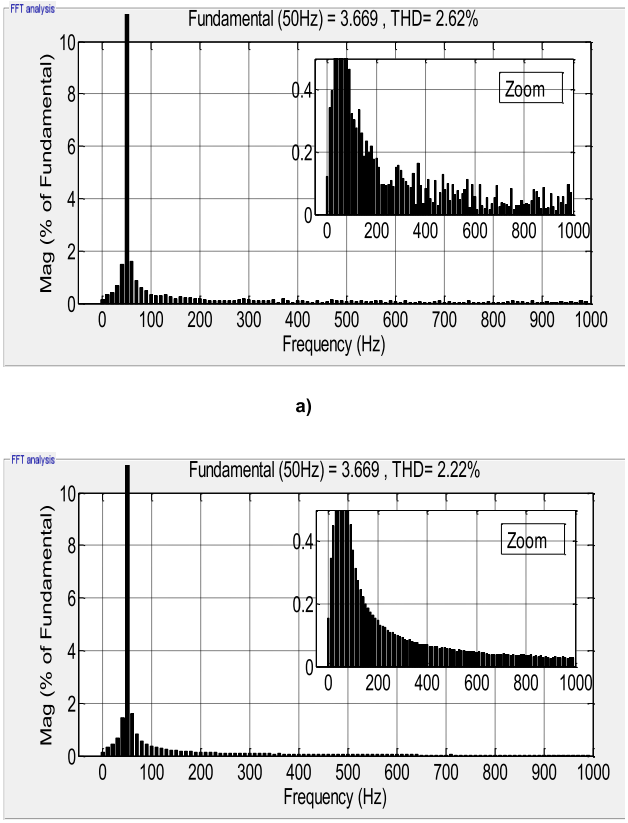

FIGURE 20. THD of stator current (Isa): (a) DPC and (b) ANN-DPC.

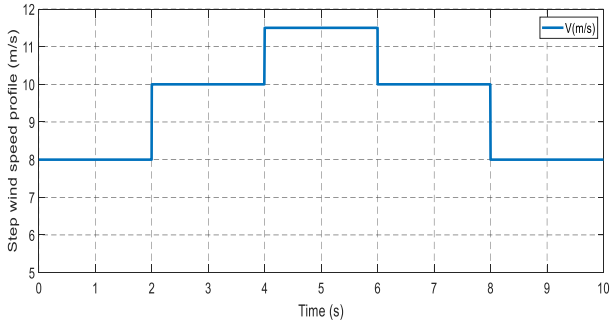

FIGURE 21. Step wind speed profile.

reference. Also, the reactive. The change in wind speed has no impact on power, however, the active power ranges from 500 W to 1500 W. The generated torque possesses the same behavior as the active power as in Figure 12. This leads to the conclusion that the torque change and the change in wind speed are related.

The rotor and the stator currents change with the change in wind speed with a maximum value of 5 A for each current as illustrated in Figures 13 and 14 respectively. A stable value of around 2.4 A is expected for the direct rotor current as given

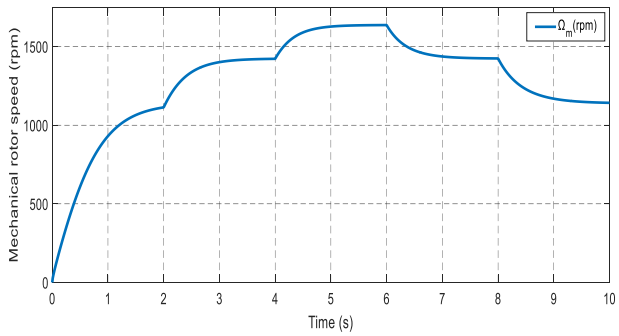

FIGURE 22. Mechanical rotor speed.

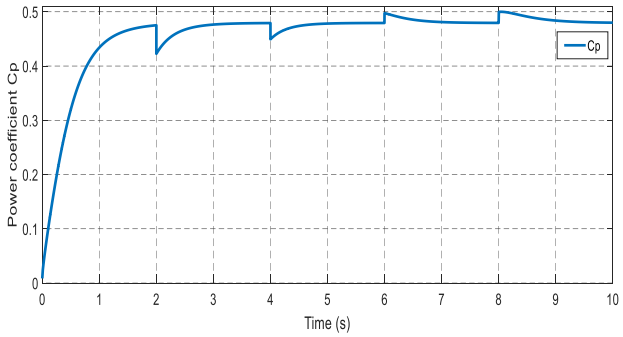

FIGURE 23. The Cp.

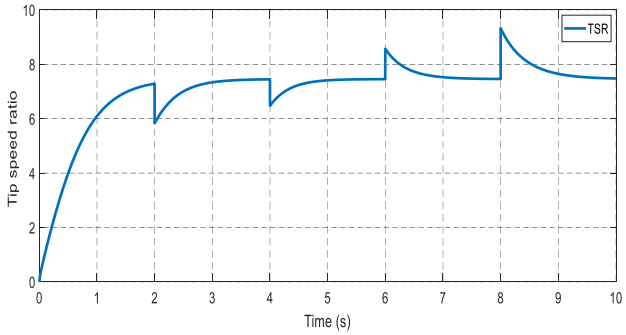

FIGURE 24. Tip speed ratio (λ).

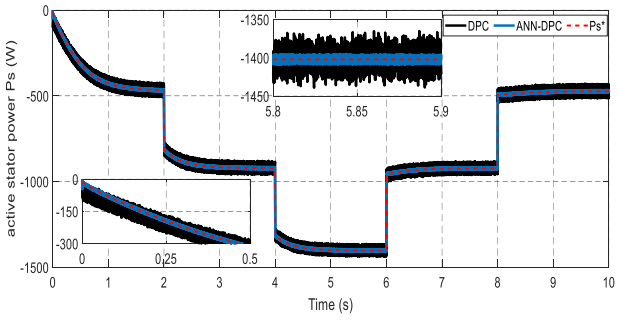

FIGURE 25. Active power.

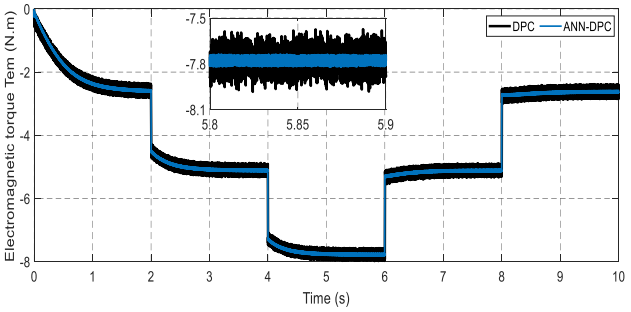

FIGURE 26. Torque.

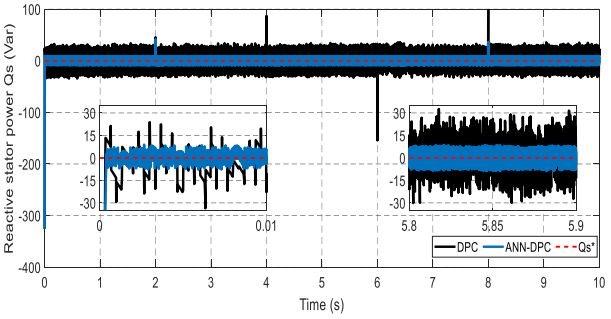

FIGURE 27. Reactive power.

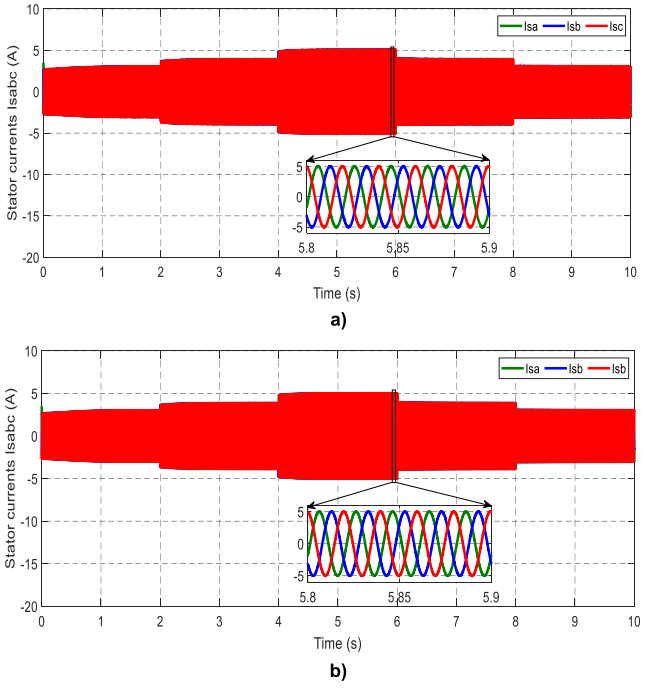

FIGURE 28. Stator currents isabc of both methods: (a) DPC and (b) ANNDPC.

in Figure 15-a. While the quadrature rotor current fluctuates in magnitude between 1.78 A and 4.2 A at its highest and lowest points, respectively as depicted in Figure 15-b. Thus, the value of the direct rotor current has a relationship with the reactive power, but the quadrature rotor current has a relationship with the active power. The power factor is around 1 with some ripples as illustrated in Figure 16. The system itself

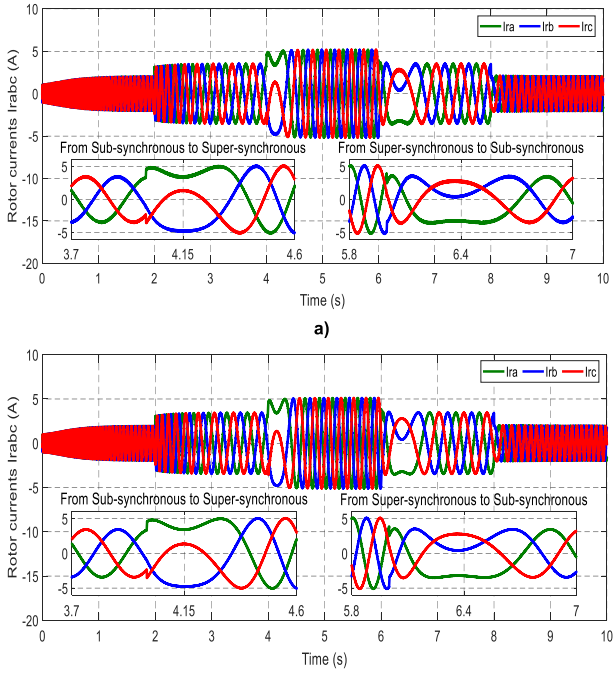

FIGURE 29. Rotor currents irabc of both methods: (a) DPC and (b) ANNDPC.

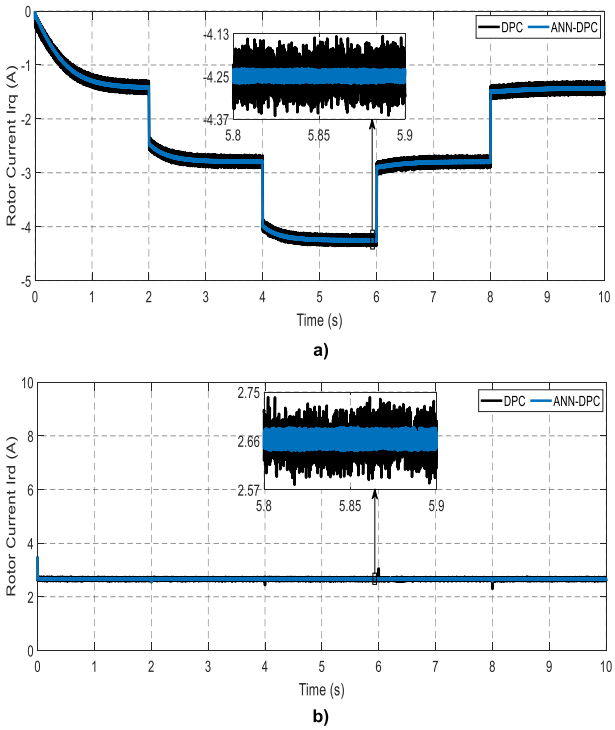

FIGURE 30. Quadrature and direct rotor currents: a) i_{rq}, b) i_{rd}.

and a change in wind speed are to blame for these ripples. When the suggested DPC-ANN technique is implemented, the stator current's THD value is around 2.22% as shown in Figure 17. This THD number is low, indicating that the

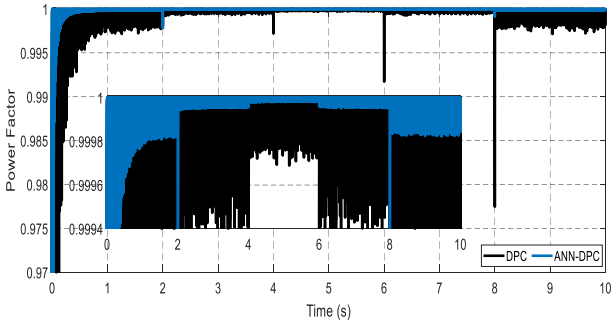

FIGURE 31. Power factor.

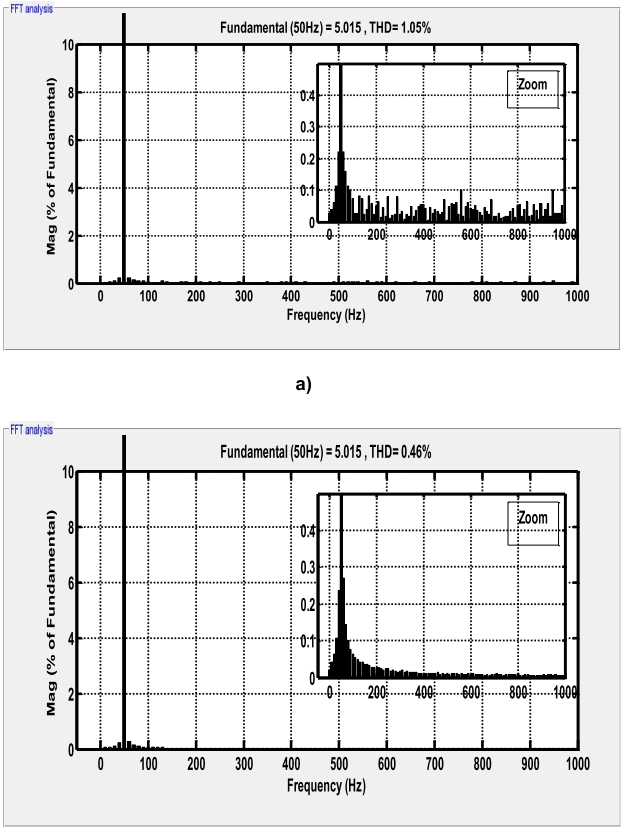

FIGURE 32. THD of current (Ias): (a) DPC and (b) ANN-DPC.

quality of the current obtained is adequate and excellent in comparison to other methods.

B. SECOND TEST CASE

This test is setpoints tracking test, where this test is used to prove the robustness of the designed strategy for the WTS. This designed wind profile makes evident the proposed strategy characteristics with respect to the sudden changes of the instructions. The proposed wind profile is shown in Figure 18, where it is changed from 8 m/s → 10 m/s →11.5 m/s → 10 m/s to 8 m/s and this is during times 2 s, 4 s, 6 s, 8 s, and

TABLE 5. Comparison of the obtained results with those reported in reference control strategies designed in the literature.

References	Strategies	THD (%)
[44]	Fuzzy sliding mode controller	3.1
[45]	DTC	3
[46]	FOC	3.7
[47]	DPC using L-filter	10.79
	DPC using LCL-filter	4.05
[48]	Second order SMC	3.13
[28]	Integral SMC	9.7
	Multi-resonant-based SMC	3.2
[49]	DPC with super twisting algorithm	1.66
[50]	Virtual flux DPC	4.2
	DPC	4.9
[51]	DTC	7.83
	DTC with neural algorithm	3.26
Proposed strategy	First test	2.22
	Second test	0.46

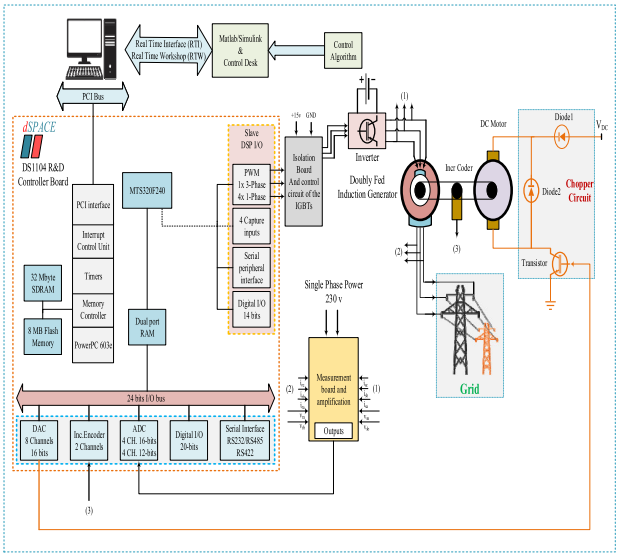

FIGURE 33. Structure of the proposed approach.

10 s, respectively. The mechanical rotor speed of the DFIG is shown in Figure 19. The shape of the mechanical rotor speed has the same shape as the change of wind speed. This applies to both the power coefficient (see Figure 20) and tip speed ratio (see Figure 21).

Active power and torque graphs have a similar form as the mechanical speed (see Figures 22 and 23). Negative active power, on the other hand, indicates that the machine is running in generator mode. The change in wind speed has no impact on the reactive power, as shown in Figure 24, where its value remains zero throughout the simulation period with small amplitude ripples.

Figures 25 and 26 represent the stator and rotor currents, respectively. Through these two figures, it can be said that

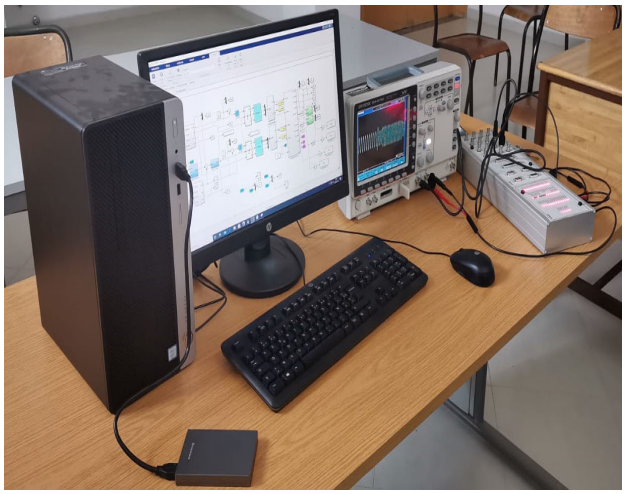

FIGURE 34. Real time implementation system.

the change in rotor and stator currents is related to the change in wind speed. As the wind speed increases, the value of the current generated by the generator increases. Figure 27 shows the quadrature and direct rotor currents of the DFIG. Direct rotor current has a constant value. On the other hand, this current takes the form of reactive power. As for the quadrature rotor current, it takes the form of active power, as we note that the value of this current increases with the increase in active power. Figure 28 shows the factor power of the DFIG. Based on this figure, the value of this factor power is about 1 with special ripples between moments 0 and 2 s. Operation with zero reactive power provides a regime with a unit power factor.

In this test, the THD of the current is 0.46 % (*respect the IEEE-519 Std*). So, this value is very low compared to the value obtained in the first test. The improvement of the THD value is about 20.72 % which is a very good ratio. The application of the proposed technique gave terrific results, and this is in the two proposed tests, and this is what appears in the results obtained.

A study comparing this work with previously done ones according to the current THD is necessary. Table 5 compares the presented study with other studies that have been published according to the THD of electric stator current. According to this table, the designed control gave a better value for the THD compared to some of the proposed methods in previously published works such as DTC and FOC strategies.

In the next part, experimental verification of the simulation results will be presented

V. IMPLEMENTING THE SUGGESTED STRATEGY

Figure 30 represents the proposed experimental work to verify the simulation results. In this work, a 1.5 KW DFIG is used in addition to a computer, Matlab software, a two-level inverter, and dSPACE carte (DS 1104). To control the inverter,

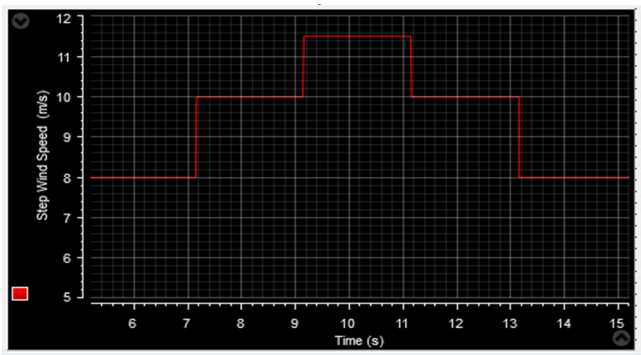

a)Step wind speed.

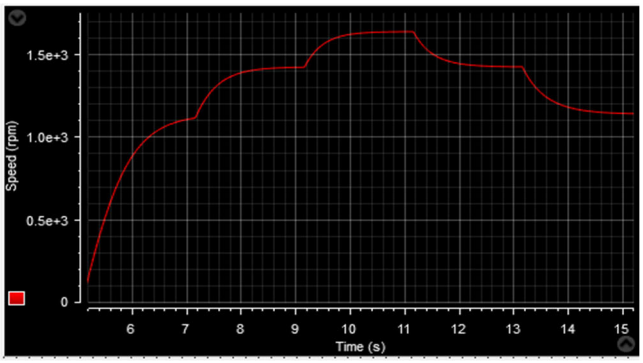

b) Generator speed.

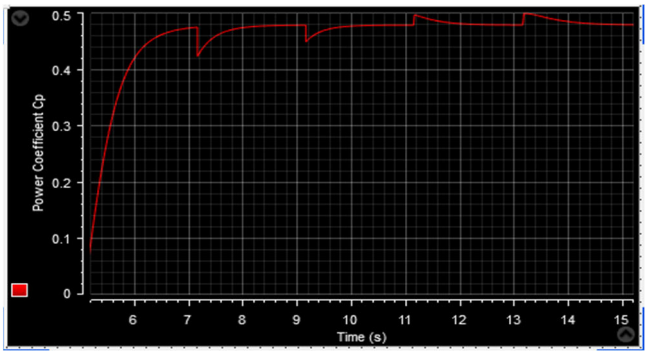

c) Power coefficient.

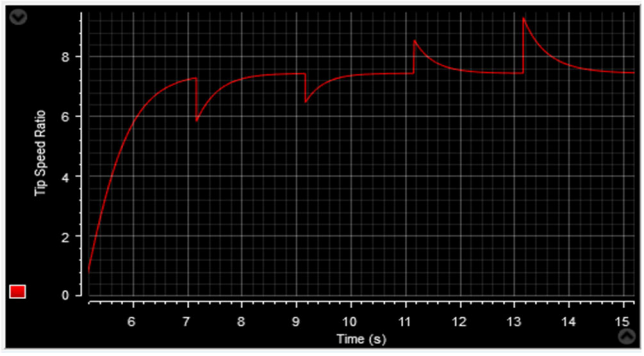

d) Tip speed ratio.

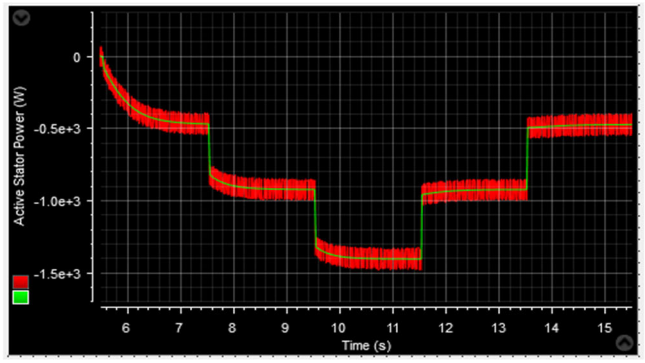

e) Active power.

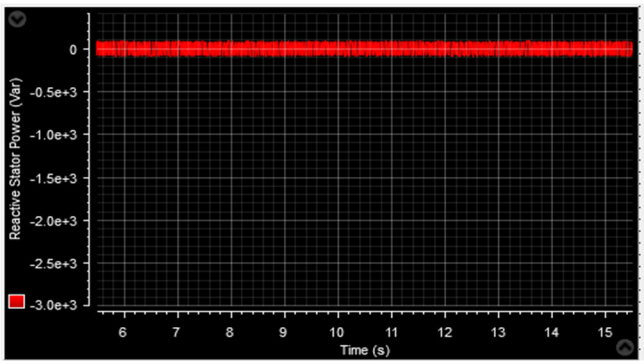

f) Reactive power.

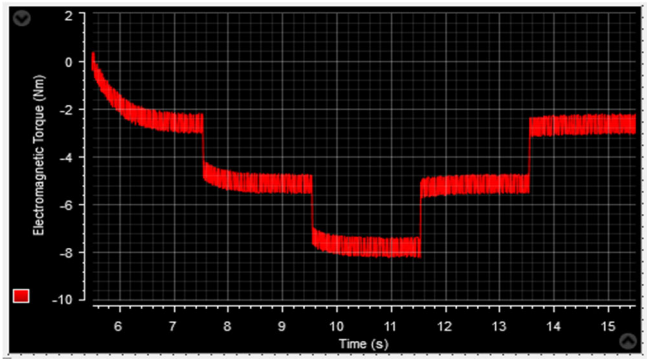

g) Torque.

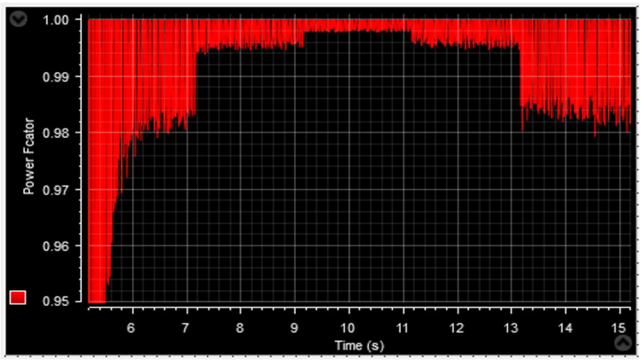

h) Power factor.

FIGURE 35. Experimental results in the case of step speed WTS.

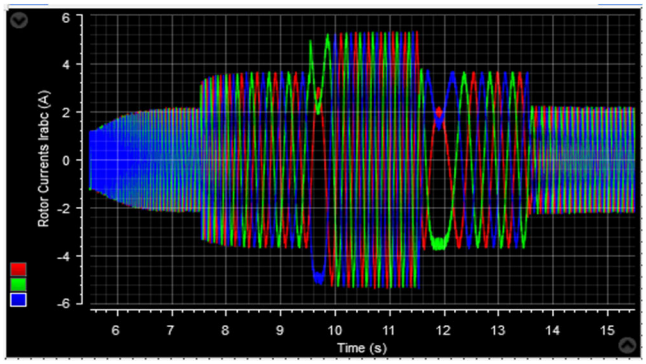

i) Rotor currents.

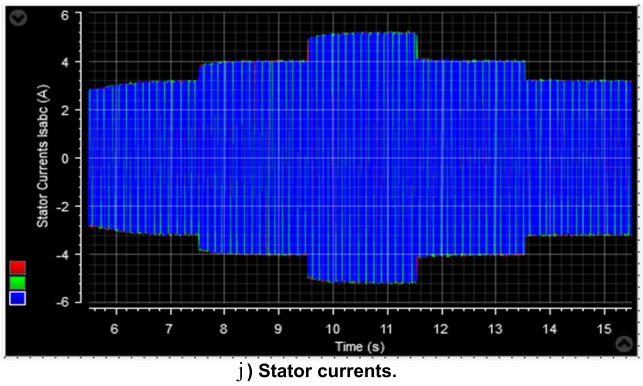

j) Stator currents.

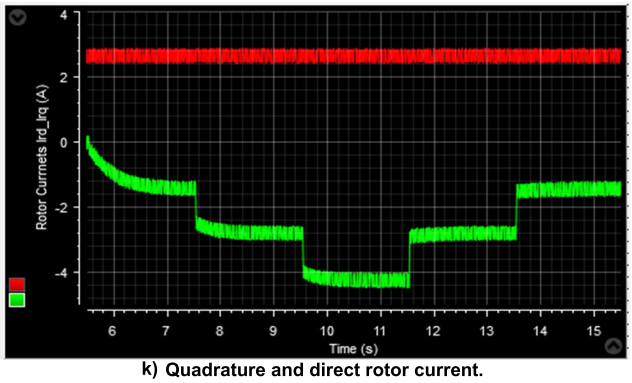

k) Quadrature and direct rotor current.

FIGURE 35. *(Continued.)* **Experimental results in the case of step speed WTS.**

the PWM strategy was used. The latter gives us a logical signal whose voltage is 5 volts, and this is in order to control the IGBTs using DSPs TMS320F240. The proposed controller is simulated via Matlab 2020. Next, the proposed control is communicated to dSPACE's DS1104 R&D controller Board. Figure 30 illustrates how the latter communicates the required signals to the inverter's IGBTs. The experimental platform validation and tests were performed using the dSPACE card and the real-time workshop tool as given in Figure 31.

In this experimental work, two tests were designed to test the durability of the designed control, and the same tests carried out in the previous section were maintained to verify the simulation results and to know the behavior of the designed control when the wind speed is changed.

VI. EXPERIMENTAL RESULTS

The outcomes of this experimental work are displayed in Figures 32 and 33, where Figure 32 represents the experimental results in the case of step wind speed, and Figure 33 represents the experimental results in the case of variable wind speed. The system's resilience against a wind level profile is demonstrated by the first test. While, the tracking effectiveness and control following a fluctuating wind profile are demonstrated by the second one. The first conclusion that can be made from these experimental findings is that they are consistent with those of the numerical simulation. Both the experimental and numerical studies yielded nearly the same behavior. In the testing, the mechanical angular speed curves precisely match the wind profile tracks. Figures 32a and 33a illustrate the wind speed profiles. Figures 32c and 33c represent the power coefficient and this is in the two tests. These two figures demonstrate how a change in the wind speed profile and an energy value are related. The λ of the WTS is shown in Figures 32d and 33d, and this is in the case of variable and step wind speed profiles, where we discover a correlation between the signal and the wind speed profiles. From these figures the tip spped ration ranges between 6 and 8.5 m/s. Figures 32e and 33e demonstrate with its mechanical reference the active stator power tracking in clear detail. The conclusion is supported by the DFIG power quality with a low rate of undulations.

Figures 32f and 33f show the reactive stator power forms with their zero-reference value. Remarkably, compared to the total power output, the reactive stator powers values in the two experiments are quite low. On the other hand, the torque of the DFIG is shown in Figure 32g and Figure 33g. In both cases, the shape of the torque is the same as the shape of the active power with the torque taking negative values, and this is because the machine is in a generator state. The value of the resulting torque changes according to the change in wind speed profiles. In addition, there is a rapid dynamic response to the torque of the generator in response to a change in the rated power.

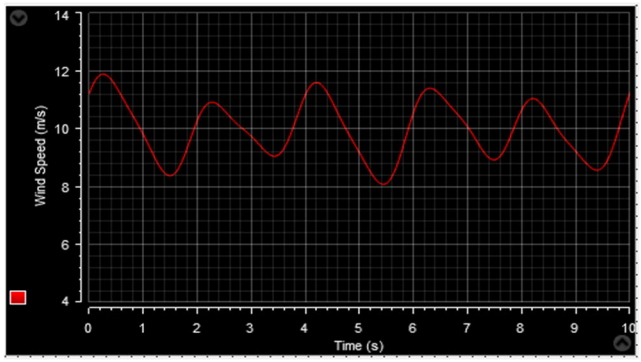

a)Wind speed profile

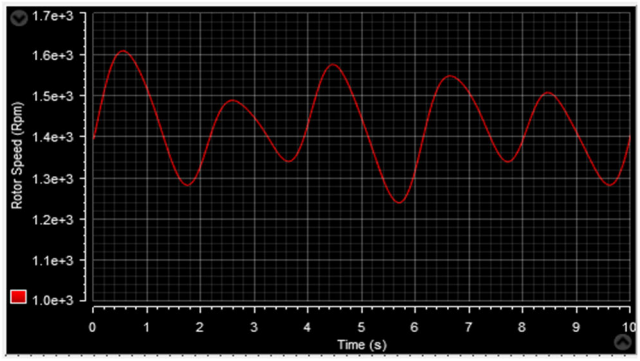

b) Generator speed.

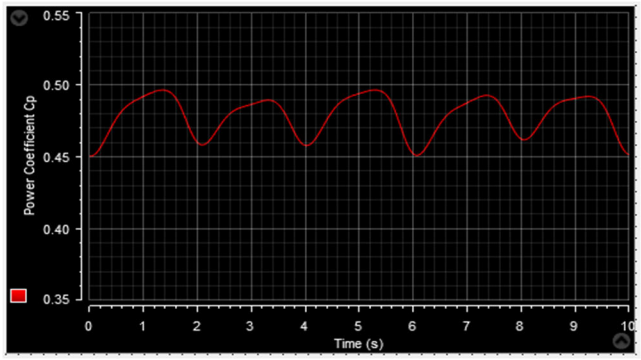

c) Power coefficient

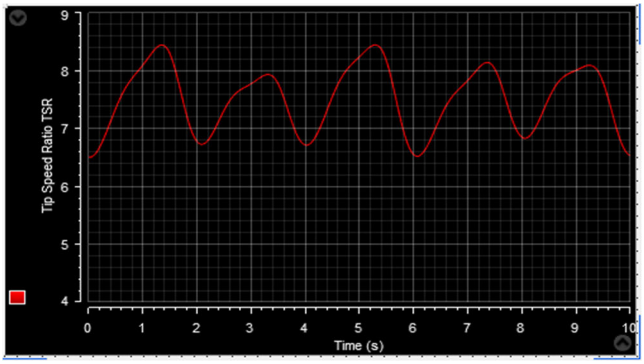

d)Tip speed ratio

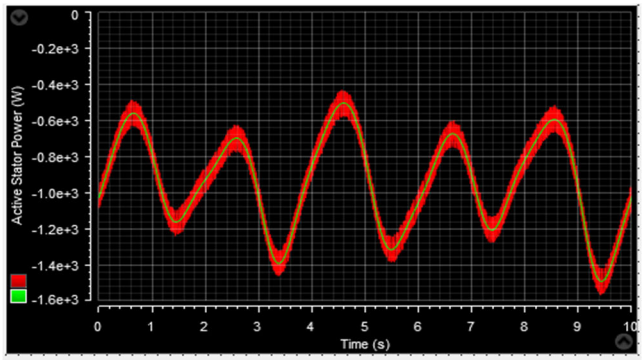

e)Active power

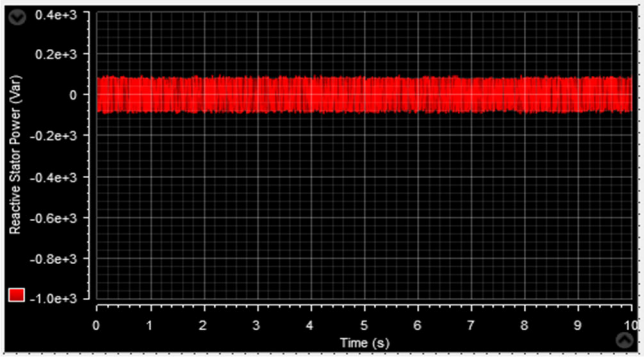

f)Reactive power

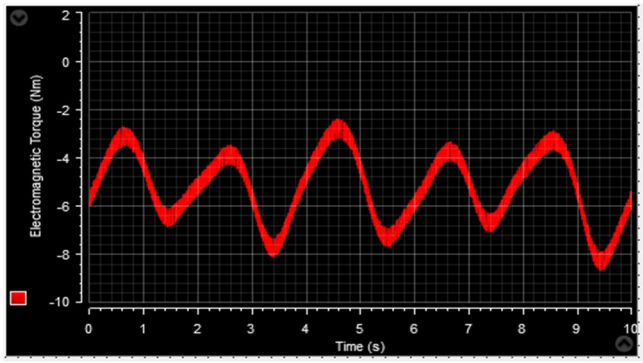

g)Torque

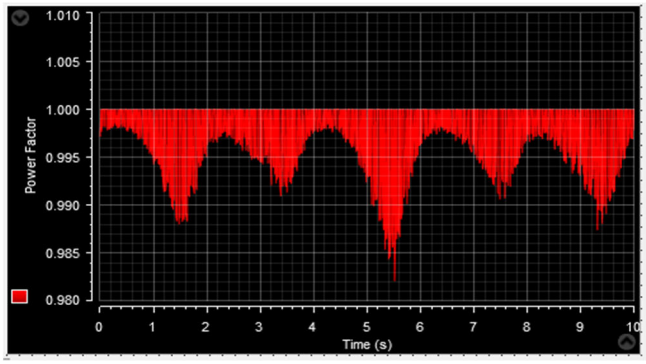

h)Power factor

FIGURE 36. Experimental results with variable speed wind turbine.

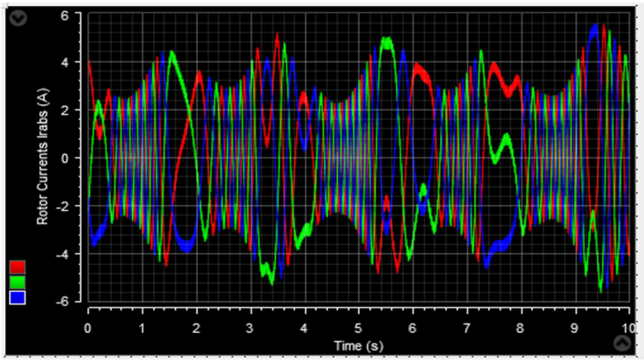

i)Rotor current

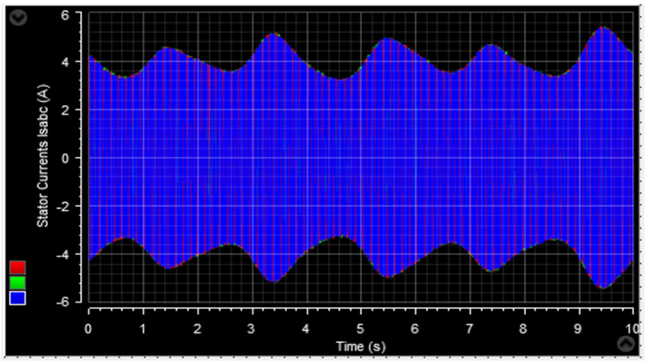

j)Stator current

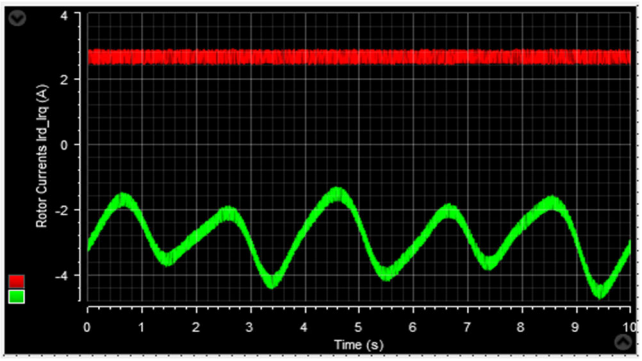

k) Quadrature and direct rotor current.

FIGURE 36. *(Continued.)* **Experimental results with variable speed wind turbine.**

Figures 32h and 33h illustrate the power factor forms of the DFIG-WTSs. From the two figures, the power factor value is approximately 1 with some faint ripples estimated at 0.02%. These ripples are caused by the system.

The three-phase rotor and stator currents profiles in the two proposed tests is shown in Figures 32k, 33k, 32l, and 33l, respectively. The stator and rotor current values are related to the system and the reference value of the active power, and they exhibit a quick dynamic reaction to changes in active power, demonstrating the efficacy of the suggested control.

The direct and quadrature rotor currents profiles in the suggested tests are indicated in Figure 32n and Figure 33n. From these figures, the direct rotor current follows the form of reactive power, where its value is zero. The length of the experimental work is independent of the wind speed profiles with small amplitude ripples. Quadrature rotor current takes the form of active power and its value changes with the change in wind speed profiles with the presence of ripples resulting from the system. These experimental results confirm the results obtained by numerical simulation.

VII. CONCLUSION

This work deals with an intelligent direct power control applied to a changing speed single-rotor WTS based-DFIG. Initially, we implement the intelligent DPC strategy concept based on the PWM strategy and the artificial neural network to operate the single-rotor wind turbine with the best characteristics. In this work, two different tests were designed to verify the characteristics of the designed intelligent DPC strategy with the PWM technique. Single-rotor wind turbine modeling, DFIG, and intelligent DPC strategy theory are developed in this work. An implementation using the DS1104 R&D Controller Board for experimental confirmation is provided and discussed. The numerical simulations and experimental results reveal the better characteristic of the designed DPC strategy in reactive/active power tracking and the quality of stator current.

The important notes of this work are:

- The proposed intelligent DPC strategy offers better characteristics in changed wind speed profile cases.
- With improved performances, the speed and pursuit of various magnitudes are guaranteed.
- Through the proposed intelligent DPC strategy, robustness against changes in the wind profile is well assured.
- The high quality of the energy efficiency and the power factor around the unit attests to the designed intelligent DPC technique efficiency.
- Based on the simulation results, the single-rotor wind turbine's static and dynamic properties are improved by the proposed intelligent DPC.

Based on experimental findings that continue to be trustworthy and comparable to those discovered in the numerical simulation, we can verify and validate the intelligent DPC approach characteristics. The current work also provides the following viewpoints:

- The incorporation of a storage unit and technical and financial WTS optimization.
- Another experimental work in the wind turbine system was driven by the DFIG. Among the suggestions are nonlinear techniques and intelligent techniques using artificial intelligence such as fuzzy logic and genetic algorithm.

REFERENCES

[1] X. Lin, K. Xiahou, Y. Liu, and Q. H. Wu, "Design and hardware-in-the-loop experiment of multiloop adaptive control for DFIG-WT," *IEEE Trans. Ind. Electron.*, vol. 65, no. 9, pp. 7049–7059, Sep. 2018, doi: 10.1109/TIE.2018.2798566.

[2] C. Hamid, A. Derouich, T. Hallabi, O. Zamzoum, M. Taoussi, S. Rhaili, and O. Boulkhrachef, "Performance improvement of the variable speed wind turbine driving a DFIG using nonlinear control strategies," *Int. J. Power Electron. Drive Syst. (IJPEDS)*, vol. 12, no. 4, p. 2470, Dec. 2021.

[3] R. Prasad and N. P. Padhy, "Synergistic frequency regulation control mechanism for DFIG wind turbines with optimal pitch dynamics," *IEEE Trans. Power Syst.*, vol. 35, no. 4, pp. 3181–3191, Jul. 2020, doi: 10.1109/TPWRS.2020.2967468.

[4] B. Habib, "A comparative study between DTC-NSTMC and DTC-FSTSMC control scheme for a DFIG-based wind turbine," *Majlesi J. Energy Manag.*, vol. 7, no. 4, pp. 43–53, 2018.

[5] B. Taheri, S. Salehimehr, and M. Sedighizadeh, "A novel strategy for fault location in shunt-compensated double circuit transmission lines equipped by wind farms based on long short-term memory," *Cleaner Eng. Technol.*, vol. 6, Feb. 2022, Art. no. 100406, doi: 10.1016/j.clet.2022.100406.

[6] M. Mosaad, N. Sabiha, A. Abu-Siada, and I. Taha, "Application of superconductors to suppress ferroresonance overvoltage in DFIG-WECS," *IEEE Trans. Energy Convers.*, vol. 37, no. 2, pp. 766–777, Jun. 2022, doi: 10.1109/TEC.2021.3126602.

[7] M. F. El-Naggar, M. I. Mosaad, H. M. Hasanien, T. A. AbdulFattah, and A. F. Bendary, "Elephant herding algorithm-based optimal PI controller for LVRT enhancement of wind energy conversion systems," *Ain Shams Eng. J.*, vol. 12, no. 1, pp. 599–608, Mar. 2021, doi: 10.1016/j.asej.2020.07.013.

[8] R. C. Bansal, "Three-phase self-excited induction generators: An overview," *IEEE Trans. Energy Convers.*, vol. 20, no. 2, pp. 292–299, Jun. 2005, doi: 10.1109/TEC.2004.842395.

[9] I. R. Y. Ahmed, K. Salah, and I. M. Mohamed, "Performance of PMSG-wind power plant during three phase faults with ANN based control of STATCOM," in *Proc. IEEE Int. Conf. Automat. Congr. Chilean Assoc. Autom. Control (ICA-ACCA)*, Santiago, Chile, Mar. 2021, pp. 1–6.

[10] C. Hamid, A. Derouich, M. Taoussi, O. Zamzoum, and A. Hanafi, "An improved performance variable speed wind turbine driving a doubly fed induction generator using sliding mode strategy," in *Proc. IEEE 2nd Int. Conf. Electron., Control, Optim. Comput. Sci. (ICECOCS)*, Dec. 2020, pp. 1–8, doi: 10.1109/ICECOCS50124.2020.9314629.

[11] R. M. Prasad and M. A. Mulla, "Mathematical modeling and position-sensorless algorithm for stator-side field-oriented control of rotor-tied DFIG in rotor flux reference frame," *IEEE Trans. Energy Convers.*, vol. 35, no. 2, pp. 631–639, Jun. 2020, doi: 10.1109/TEC.2019.2956255.

[12] A. Ardjal, M. Bettayeb, R. Mansouri, and A. Mehiri, "Nonlinear synergetic control approach for DC-link voltage regulator of wind turbine DFIG connected to the grid," in *Proc. 5th Int. Conf. Renew. Energy, Gener. Appl. (ICREGA)*, Feb. 2018, pp. 94–97, doi: 10.1109/ICREGA.2018.8337639.

[13] H. Chojaa, A. Derouich, M. Taoussi, O. Zamzoum, and M. Yessef, "Optimization of DFIG wind turbine power quality through adaptive fuzzy control," in *Digital Technologies and Applications*. vol. 211. Cham, Switzerland: Springer, 2021, doi: 10.1007/978-3-030-73882-2_113.

[14] A. Alhejji and M. I. Mosaad, "Performance enhancement of grid-connected PV systems using adaptive reference PI controller," *Ain Shams Eng. J.*, vol. 12, no. 1, pp. 541–554, Mar. 2021, doi: 10.1016/j.asej.2020.08.006.

[15] H. Benbouhenni and N. Bizon, "Improved rotor flux and torque control based on the third-order sliding mode scheme applied to the asynchronous generator for the single-rotor wind turbine," *Mathematics*, vol. 9, no. 18, p. 2297, Sep. 2021, doi: 10.3390/math9182297.

[16] C. Lascu, I. Boldea, and F. Blaabjerg, "A modified direct torque control for induction motor sensorless drive," *IEEE Trans. Ind. Appl.*, vol. 36, no. 1, pp. 122–130, Jan./Feb. 2000, doi: 10.1109/28.821806.

[17] Y. Sahri, S. Tamalouzt, S. L. Belaid, S. Bacha, N. Ullah, A. A. A. Ahamdi, and A. N. Alzaed, "Advanced fuzzy 12 DTC control of doubly fed induction generator for optimal power extraction in wind turbine system under random wind conditions," *Sustainability*, vol. 13, no. 21, p. 11593, Oct. 2021, doi: 10.3390/su132111593.

[18] A. Yousefi-Talouki, S. Zalzar, and E. Pouresmaeil, "Direct power control of matrix converter-fed DFIG with fixed switching frequency," *Sustainability*, vol. 11, no. 9, p. 2604, May 2019, doi: 10.3390/su11092604.

[19] M. A. Mossa, H. Echeikh, A. A. Z. Diab, and N. V. Quynh, "Effective direct power control for a sensor-less doubly fed induction generator with a losses minimization criterion," *Electronics*, vol. 9, no. 8, p. 1269, Aug. 2020, doi: 10.3390/electronics9081269.

[20] H. Chojaa, A. Derouich, S. E. Chehaidia, O. Zamzoum, M. Taoussi, and H. Elouatouat, "Integral sliding mode control for DFIG based WECS with MPPT based on artificial neural network under a real wind profile," *Energy Rep.*, vol. 7, pp. 4809–4824, Nov. 2021, doi: 10.1016/j.egyr.2021.07.066.

[21] H. Chojaa, A. Derouich, M. Taoussi, S. Chehaidia, O. Zamzoum, M. Mosaad, A. Alhejji, and M. Yessef, "Nonlinear control strategies for enhancing the performance of DFIG-based WECS under a real wind profile," *Energies*, vol. 15, no. 18, p. 6650, Sep. 2022, doi: 10.3390/en15186650.

[22] R. A. De Marchi, P. S. Dainez, F. J. Von Zuben, and E. Bim, "A multilayer perceptron controller applied to the direct power control of a doubly fed induction generator," *IEEE Trans. Sustain. Energy*, vol. 5, no. 2, pp. 498–506, Apr. 2014, doi: 10.1109/TSTE.2013.2293621.

[23] F. Amrane, A. Chaiba, B. Babes, and S. Mekhilef, "Design and implementation of high performance field oriented control for grid-connected doubly fed induction generator via hysteresis rotor current controller," *Rev. Roum. Sci. Techn.-Electrotechn. Et Energ*, vol. 61, no. 4, pp. 319–324, 2016.

[24] I. Erazo-Damian, J. M. Apsley, R. Perini, M. F. Iacchetti, and G. D. Marques, "Stand-alone DFIG FOC sensitivity and stability under mismatched inductances," *IEEE Trans. Energy Convers.*, vol. 34, no. 2, pp. 860–869, Jun. 2019, doi: 10.1109/TEC.2018.2869286.

[25] L. Xiong, P. Li, H. Li, and J. Wang, "Sliding mode control of DFIG wind turbines with a fast exponential reaching law," *Energies*, vol. 10, no. 11, p. 1788, Nov. 2017, doi: 10.3390/en10111788.

[26] J. A. Cortajarena, O. Barambones, P. Alkorta, and J. Cortajarena, "Grid frequency and amplitude control using DFIG wind turbines in a smart grid," *Mathematics*, vol. 9, no. 2, p. 143, Jan. 2021, doi: 10.3390/math9020143.

[27] A. Susperregui, J. M. Herrero, M. I. Martinez, G. Tapia-Otaegui, and X. Blasco, "Multi-objective optimisation-based tuning of two second-order sliding-mode controller variants for DFIGs connected to non-ideal grid voltage," *Energies*, vol. 12, no. 19, p. 3782, Oct. 2019, doi: 10.3390/en12193782.

[28] Y. Quan, L. Hang, Y. He, and Y. Zhang, "Multi-resonant-based sliding mode control of DFIG-based wind system under unbalanced and harmonic network conditions," *Appl. Sci.*, vol. 9, no. 6, p. 1124, Mar. 2019, doi: 10.3390/app9061124.

[29] G. Brando, A. Dannier, and I. Spina, "Performance analysis of a full order sensorless control adaptive observer for doubly-fed induction generator in grid connected operation," *Energies*, vol. 14, no. 5, p. 1254, Feb. 2021, doi: 10.3390/en14051254.

[30] E. Hernández-Mayoral, E. Dueñas-Reyes, R. Iracheta-Cortez, E. Campos-Mercado, V. Torres-García, and R. Uriza-Gosebruch, "Modeling and validation of the switching techniques applied to back-to-back power converter connected to a DFIG-based wind turbine for harmonic analysis," *Electronics*, vol. 10, no. 23, p. 3046, Dec. 2021, doi: 10.3390/electronics10233046.

[31] M. Bouderbala, B. Bossoufi, O. Deblecker, H. A. Aroussi, M. Taoussi, A. Lagrioui, S. Motahhir, M. Masud, and F. A. Alraddady, "Experimental validation of predictive current control for DFIG: FPGA implementation," *Electronics*, vol. 10, no. 21, p. 2670, Oct. 2021, doi: 10.3390/electronics10212670.

[32] A. Khan, X. M. Hu, M. A. Khan, and P. Barendse, "Doubly fed induction generator open stator synchronized control during unbalanced grid voltage condition," *Energies*, vol. 13, no. 12, p. 3155, Jun. 2020, doi: 10.3390/en13123155.

[33] M. Abdelrahem, C. Hackl, R. Kennel, and J. Rodriguez, "Low sensitivity predictive control for doubly-fed induction generators based wind turbine applications," *Sustainability*, vol. 13, no. 16, p. 9150, Aug. 2021, doi: 10.3390/su13169150.

[34] M. Abdelrahem, C. M. Hackl, and R. Kennel, "Limited-position set model-reference adaptive observer for control of DFIGs without mechanical sensors," *Machines*, vol. 8, no. 4, p. 72, Nov. 2020, doi: 10.3390/machines8040072.
[35] J. Hussain and M. K. Mishra, "An efficient wind speed computation method using sliding mode observers in wind energy conversion system control applications," *IEEE Trans. Ind. Appl.*, vol. 56, no. 1, pp. 730–739, Jan. 2020, doi: 10.1109/TIA.2019.2942018.
[36] J. R. De Oliveira and A. L. Andreoli, "Wind turbine emulator: A tool for experimental and computational study," *IEEE Latin Amer. Trans.*, vol. 19, no. 11, pp. 1832–1839, Nov. 2021, doi: 10.1109/TLA.2021.9475616.
[37] K. Fischer, "Reliability of power converters in wind turbines: Exploratory analysis of failure and operating data from a worldwide turbine fleet," *IEEE Trans. Power Electron.*, vol. 34, no. 7, pp. 6332–6344, Jul. 2019, doi: 10.1109/TPEL.2018.2875005.
[38] M. Fdaili, A. Essadki, M. Nadour, and T. Nasser, "Comparative study of MPPT and pitch angle control strategies for a wind energy conversion system," in *Proc. Int. Renew. Sustain. Energy Conf. (IRSEC)*, Dec. 2017, pp. 300–310.
[39] R. M. Prasad and M. A. Mulla, "Rotor position-sensorless algorithms for direct power control of rotor-tied DFIG," *IEEE Trans. Power Electron.*, vol. 36, no. 6, pp. 6213–6217, Jun. 2021, doi: 10.1109/TPEL.2020.3040705.
[40] B. Hu, H. Nian, J. Yang, M. Li, and Y. Xu, "High-frequency resonance analysis and reshaping control strategy of DFIG system based on DPC," *IEEE Trans. Power Electron.*, vol. 36, no. 7, pp. 7810–7819, Jul. 2021, doi: 10.1109/TPEL.2020.3045860.
[41] S. Gao, H. Zhao, Y. Gui, D. Zhou, and F. Blaabjerg, "An improved direct power control for doubly fed induction generator," *IEEE Trans. Power Electron.*, vol. 36, no. 4, pp. 4672–4685, Apr. 2021, doi: 10.1109/TPEL.2020.3024620.
[42] X. Wang, D. Sun, and Z. Q. Zhu, "Resonant-based backstepping direct power control strategy for DFIG under both balanced and unbalanced grid conditions," *IEEE Trans. Ind. Appl.*, vol. 53, no. 5, pp. 4821–4830, Sep. 2017, doi: 10.1109/TIA.2017.2700280.
[43] S. Gao, H. Zhao, Y. Gui, D. Zhou, V. Terzija, and F. Blaabjerg, "A novel direct power control for DFIG with parallel compensator under unbalanced grid condition," *IEEE Trans. Ind. Electron.*, vol. 68, no. 10, pp. 9607–9618, Oct. 2021, doi: 10.1109/TIE.2020.3022495.
[44] W. Ayrir, M. Ourahou, B. El Hassouni, and A. Haddi, "Direct torque control improvement of a variable speed DFIG based on a fuzzy inference system," *Math. Comput. Simul.*, vol. 167, pp. 308–324, Jan. 2020, doi: 10.1016/j.matcom.2018.05.014.
[45] Z. Boudjema, R. Taleb, Y. Djeriri, and A. Yahdou, "A novel direct torque control using second order continuous sliding mode of a doubly fed induction generator for a wind energy conversion system," *Turkish J. Electr. Eng. Comput. Sci.*, vol. 25, no. 2, pp. 965–975, 2017.
[46] F. Amrane and A. Chaiba, "A novel direct power control for grid-connected doubly fed induction generator based on hybrid artificial intelligent control with space vector modulation," *Rev. Sci. Techn.-Electrotechn. Et Energ.*, vol. 61, no. 3, pp. 263–268, 2016.
[47] M. M. Alhato and S. Bouallégue, "Direct power control optimization for doubly fed induction generator based wind turbine systems," *Math. Comput. Appl.*, vol. 24, no. 3, p. 77, Aug. 2019, doi: 10.3390/mca24030077.
[48] A. Yahdou, B. Hemici, and Z. Boudjema, "Second order sliding mode control of a dual-rotor wind turbine system by employing a matrix converter," *J. Elect. Eng.*, vol. 16, no. 3, pp. 1–11, 2016.
[49] I. Yaichi, A. Semmah, P. Wira, and Y. Djeriri, "Super-twisting sliding mode control of a doubly-fed induction generator based on the SVM strategy," *Periodica Polytechnica Electr. Eng. Comput. Sci.*, vol. 63, no. 3, pp. 178–190, Jun. 2019.
[50] N. A. Yusoff, A. M. Razali, K. A. Karim, T. Sutikno, and A. Jidin, "A concept of virtual-flux direct power control of three-phase AC–DC converter," *Int. J. Power Electron. Drive Syst.*, 2017, vol. 8, no. 4, pp. 1776–1784, doi: 10.11591/ijpeds.v8.i4.pp1776-1784.
[51] M. Said, A. Derouich, O. N. El, and M. M. El, "Enhancement of the direct torque control by using artificial neuron network for a doubly fed induction motor," *Intell. Syst. Appl.*, vol. 13, Jan. 2022, Art. no. 200060, doi: 10.1016/j.iswa.2022.200060.